Wet avalanches: long-term evolution in the Western Alps under climate and human forcing

Laurent Fouinat[1], Pierre Sabatier[1], Fernand David[2], Xavier Montet[3], Philippe Schoeneich[4], Eric Chaumillon[5], Jérôme Poulenard[1], Fabien Arnaud[1]

[1]EDYTEM, University Savoie Mont Blanc, CNRS, 73376 Le Bourget du Lac Cedex, France
[2]CEREGE, University Aix-Marseille, 13545 Aix en Provence, France
[3]University of Geneva Department of Radiology and Medical Informatics Genève, CH-1211, Switzerland
[4]IUGA, University Grenoble Alpes, 38100 Grenoble, France
[5]LIENSs University of La Rochelle, 17 000 La Rochelle, France

Correspondence to: Laurent Fouinat (Laurent.fouinat@gmail.com)

Abstract. Understanding wet avalanche intensity and the role of past environmental changes on wet avalanche occurrence is a main concern especially in the context of a warming climate and accelerated environmental mutations. Avalanches are closely related to fast cryosphere changes and may cause major threats to human society. Here, we used the sedimentary archive of the alpine Lake Lauvitel (western French Alps) to establish the first long-term avalanche record in this Alpine region. For this purpose, we used a novel CT scan methodology that allows the precise identification of coarse material – from sand to pebble - transported to the lake and embedded within the finer continuous sedimentation. We identified a total of 166 deposits over the last 3300 yrs cal. BP. In parallel, a detailed pollen analysis gave an independent record of environmental changes. Based on modern observation, lake monitoring, seismic investigations and sedimentological evidences, coarse material deposits were attributed to wet avalanche events. Our results highlight the effect of vegetation cover on the avalanche hazard while a period of strong frequency increase occurred after 780 yrs cal. BP. In Lake Lauvitel, this period corresponds to a major forest clearance induced by the rise of human land-use. Climate forcing on the avalanche hazard was investigated before and after the vegetation shift. On a multi-centennial scale, wet avalanches preferably occur during periods of larger glacier extent, in which higher winter precipitations probably generate a sufficiently thick snow cover. On a sub-centennial scale, avalanches are more frequent during periods of relative warming, resulting in a destabilisation of the same snow cover in spring season. Our results highlight as well the role of forest cover to mitigate wet snow avalanches occurrence. In the context of predicted warmer temperatures, this study raises the question of whether a wet avalanche hazard increase may be expected in the near future especially at higher altitudes.

1 Introduction

Avalanche hazard is one of the major threats to human societies in mountain environments, and in the context of warmer temperatures, avalanche occurrence patterns will likely be modified by a reduction of dry snowpack and an increase in wet snowpack (Castebrunet et al., 2014). Complex meteorological conditions over a period of days to several weeks control the

5 snowpack stabilization, and occurrence of wet avalanches highly depends on temperature conditions because more likely to occur when the average daily temperature exceeds 0°C (Baggi and Schweizer, 2009). Furthermore, regional models are predicting an increase in wet avalanche activity for the coming decades, mostly related to an earlier occurrence in the spring season and an avalanche risk expected at higher altitude (Lazar and Williams, 2008; Castebrunet et al., 2014). In this study, we focus on wet avalanches, considered as dense flows characterized by wet snow which liquid water content is around 3-15

10 Vol.% (Fierz et al., 2009). Those glide on the substratum and are able to transport coarse detrital sediments such as gravels and pebbles (Luckman, 1977; Moore et al., 2013). Within the last 40 years, snow cover duration has decreased, and the number of wet snow avalanches in the spring time is increasing (Valt and Paola, 2013; Ancey and Bain, 2015). For risk management, it is crucial to understand processes favouring the occurrence of such events over long periods. In this context, it could be valuable to develop a natural archive in which those events and their potential triggering factors are recorded. In

15 that aim, most studies have used dendrochronology and tree-ring growth disturbances to date and identify avalanche events (Corona et al., 2010; Martin and Germain, 2016). This methodology i) allows annual resolution dating, ii) estimates avalanche extension, and iii) provides natural chronicles of up to several centuries. However, long-scale records of avalanche hazards remain scarce. Multiple millennial-scale avalanche records on a regional basis would improve the understanding of avalanche occurrence and allow long-term comparison with existing climate and environmental change records (Stoffel and

20 Bollschweiler, 2008). In addition, natural vegetation cover in the Alps was modified by human practices (Touflan et al., 2010), and potential tree-ring-based avalanche records may have been altered. In this context, lake sediment archives can provide an alternative, with the advantage of providing i) longer archives and ii) the coeval record of other environmental parameters such as erosion or vegetation dynamics. However, to record avalanche events in lake sediment, the watershed connected to the lake system must present steep slopes and corridors that can channel sediment to the lake. The detection of

25 avalanche deposits in lake sediment is based on the identification of poorly sorted sediment with coarse grains in a fine matrix (Nesje et al., 2007; Vasskog et al., 2011), as opposed to debris flow deposits, characterized by fining upward trend with a coarse grain base (Iverson, 1997; Sletten et al., 2003). Classically, those coarse grains were identified using a wet sieving technique, which is still a time-consuming and destructive method. Lake Lauvitel is located in the western French Alps and has preserved gravels originating from wet avalanches within its sediment. We based our avalanche chronicle on a

30 novel CT-scan methodology to precisely reference and quantify the coarse grains in the lake sediment (Fouinat et al., 2017a). This avalanche chronicle includes the flood deposit occurrence and palynological analysis over the last 3300 cal. yrs BP, allowing us to discuss the respective impact of past human and climate forcing on long-term wet avalanche occurrence patterns.

2 Material and methods

2.1. Study area

Lake Lauvitel (44,96667° N, 6,05000° E), 1500 m.a.s.l. (meters above sea level) is located in the western French Alps, 35 km southeast of Grenoble (Fig. 1). The total drainage area is approximately 15.1 km², and the lake surface covers 0.35 km². This lake was formed by a natural dam created by a large rockslide dated by Beryllium exposure age back to 4.7±0.4 Kyr [10]Be (Delunel et al., 2010). The porous outlet through the dam induces a seasonal water table height variation of approximately 20 meters, with a maximum height reached in July (61 m) and a minimum in May (40 m). From late December to early May, the lake surface is frozen, and snow covers most of the drainage area. The maximum watershed elevation is 3169 m.a.s.l., and the bedrock is mainly composed of granite and gneiss with minor outcrops of Triassic limestone. The Petit Embernard torrent drains a regularly sloped (10°) subcatchment, and a large delta has formed at the lake entrance. Two smaller streams (Plan Vianney and Héritère) are present on the western side of the lake and are characterized by steep slopes of approximately 40°. Three gullies (C1, C2, and C3) are also present, and snow accumulation resulting from avalanche deposition is sometimes observed during the spring season at the bottom of the gullies (Fouinat et al., 2017a). Current vegetation cover in the watershed is composed of a spruce forest present around only the deltaic form south of the lake. The western part of the watershed exhibits vegetation composed of shrubs (*Juniperus* and *Alnus*) especially in the vicinity of the avalanche corridors of the C2 and C3 gullies. Based on direct observations in the western part of the watershed, shrubs can also be associated with isolated trees, mostly *Abies* and *Pinus Cembra*. The higher altitude vegetation can be described as an alpine lawn, especially in the southern part of the watershed. The lake is situated in the restricted area of Ecrins National Park, and since 1995, the southern part of the watershed has been one of the only integrally protected areas in France, where human presence is strictly prohibited, allowing for the regrowth of natural vegetation.

2.2 Lake Coring

A 15.46m long sediment core was extracted in July 2011 using a Uwitec piston coring device installed on a coring platform. The core was retrieved from the deepest part of the lake at 61 m depth (6,06258333°E; 44,96898333°N). The sediment sequence LAU11 (IGSN: IEFRA007I, codes refer to an open international database, www.geosamples. org) was composed of five overlapping coring holes, LAU11-01, LAU11-02, LAU11-03, LAU11-04, LAU11-07 respectively made of 9, 2, 1, 1 and 5 sections. The high number of coring holes is due to the presence of gravel and stones layers, sometimes impenetrable, but insures a 1-m sediment overlap providing a continuous record. A short gravity core (LAU11P2) was also taken to provide a well preserved water-sediment interface that was subsequently correlated to the composite sequence. Sediment cores were split into two halves at the EDYTEM laboratory. Each section was described in detail and pictures were taken at a 20-pixel mm^{-1} resolution. Lithological description of the sequence allowed the identification of different sedimentary facies. The composite sediment sequence named LAU11 was built using distinct marker layers from the overlapping section of parallel holes.

2.3 High resolution seismic survey

In September 2012, we acquired about 15 km of high resolution seismic profiles in Lake Lauvitel (28 profiles Fig. 3). Positioning of seismic profiles was obtained using a GPS system with its antenna directly mounted on the seismic profiler. The seismic profiler was the IKB Seistec, a boomer plate associated with a line-in-cone short streamer (Simpkin and Davis, 1993). This seismic profiler dedicated to shallow waters allowed us to obtain profiles in the lake system. The band pass frequency was 1 to 10 kHz giving a vertical resolution of about 20 cm. A 50 J power supply was selected. The shot interval was 250 ms, corresponding to distance between adjacent traces of about 25 cm for a ship speed of about 2 knots.

2.4 Sedimentary analysis

The grain-size distribution on most of the identified layers was measured with a 5-mm sampling step using a Malvern Mastersizer 800 laser particule sizer. Ultrasonics were used to dissociate particles and to avoid flocculation. We then used the median (Q50) and the coarsest (Q90) fractions, in addition to the sorting parameter to characterize interbedded deposits (Mulder et al., 2001; Passega, 1964; Vasskog et al., 2011; Wilhelm et al., 2015).

2.5 CT scan imagery

Several layers of gravel-sized mineralogic particles were identified in the LAU11 sediment sequence. To characterize the coarse fraction, a CT scan analysis was performed on split sediment cores at the Hopitaux Universitaires de Genève (HUG) following the methodology from Fouinat et al., (2017a). The entire composite sediment sequence was divided into 15445 frames of 1-mm thickness. Image resolution parameter was set to 512x512 pixels, with a pixel corresponding to 500x500 µm. Images were then stacked using ImageJ FIJI application (Schindelin et al., 2012) to obtain 0.25 mm^3 resolution voxels (i.e., volumetric pixels) for the sediment sequence. Image treatments were performed using the 3D Object Counter plugin (Bolte and Cordelieres, 2006). First, we isolated the highest density values recovered in the sediment cores in order to identify the densest sedimentary elements corresponding to the outlier presence of gravel size mineralogic element within the finer sediment matrix. The 3D Object counter was used to reconstruct the precise depth in a 3D coordinate system (Fouinat et al., 2017a).

2.6 Palynological analysis

In total, 32 samples of 1 cm^3 of sediment were taken along the sequence between 0.09 and 15.41 m at variable intervals within the event-free sedimentation for better grain preservation and more accurate statistical representation. The samples were prepared for pollen analysis following the standard acetylation and hydrofluoric acid method (Faegri et al., 1989). The pollen sum was at least 500 grains. The software package GpalWin (Goeury, 1988) was used to construct pollen diagrams.

2.7 Chronology

The chronology of the Lake Lauvitel sediment sequence is based on short-lived radionuclide ^{226}Ra, ^{210}Pb, ^{241}Am, and ^{137}Cs (Fouinat et al., 2017a), with non-regular sampling following facies distinction avoiding thick beds. In complement, we selected 19 samples on terrestrial plant macroremains for ^{14}C measurements. Those were performed by accelerator mass

5   spectrometer (AMS) at the Poznan Radiocarbon Laboratory and at the Laboratoire de Mesure ^{14}C (LMC14) ARTEMIS at the CEA (Atomic Energy Commission) Institute at Saclay (Table 1). The ^{14}C ages were converted to 'calendar' years using the calibration curve IntCal13 (Reimer et al., 2013). The age–depth model was then generated using R software and the R-code package 'Clam' version 2.2 (Blaauw, 2010).

3 Results

10   ### 3.1 Seismic survey

The Lauvitel Lake basin consists of a shallow northern area and a deep southern area. The northern area displays sediment accumulation of less than 2 ms twtt lying on an acoustic basement, whereas the southern basin exhibits a succession of sub-horizontal medium to strong amplitude reflectors increasingly discontinuous with depth (Fig. 2). The deepest strong amplitude reflector is lying at approximately 18.8 ms twtt. However, clear identification of substratum upper surface was not

15   possible probably related to signal attenuation. The 03-6 profile shot along a W-E direction shows two units (Fig 2 in red) pinching out toward the east, displaying a chaotic internal configuration and multiple reflectors downlapping on two strong amplitude sub-horizontal reflectors lying at 11.8 and 17.3 ms twtt. Thinner units pinching out basinward (Fig 2 in blue) are based by sub-horizontal and strong amplitude reflectors and topped by and undulated surface displaying convex-up reflectors.

20   ### 3.2 Sedimentology

3.2.1 Core description and lithology

Based on macroscopic observations, grain size analysis and CT scan imagery we identified four different facies in the LAU11 sediment sequence. F1 is composed of homogeneous to finely laminated silty mud. Two subclasses can be distinguished according to grain size parameters, F1A is characterized by a homogeneous median value (Q50) around 13.5

25   μm and low sorting values (<2.7) (Fig. 3a).

On the contrary, F1G characterized by the presence coarse grains and higher sorting values (> 2.6). In F1G, CT high density filter analysis reveals the presence of multiple pebbles disposed in layers parallel to surrounding lamination, expressed as a count of gravels in a 5 mm sediment thickness (Fig. 3a). In this figure, an example of F1G layer is shown where 14 individual pebbles were identified. Whereas most of the 166 F1G layers had thicknesses comprised between 0.2 and 5.4 cm,

30   we found three outstanding layers of 48.5, 52 and 54 cm respectively at 6.35, 8.49 and 14.58 meters of depth. The 52 cm

layer (Fig. 3b) exhibits a multimodal grain size distribution characterized by median values of 38 to 114 μm, coarser percentile of 313 to 374 μm and bad sorting values (>3.4), with no indication of a fining upward trend. Macroscopic observations revealed the presence of multiple coarse grains in this layer, supported by CT high density filter identification of numerous dense objects (gravels and pebbles). The corresponding graph of pebble counts has identified a total of 355 individuals, but based on the CT images the number of individuals is more likely to be higher. The difference could be due to the proximity of individual pebbles making difficult to identify them separately by image analysis. The multi-modal grain size distribution indicates the input of a coarse sandy fraction accompanied by pebbles within a fine sediment matrix in accordance with a previous study on the upper sediment sequence of lake Lauvitel (Fouinat et al., 2017a). Additionally, we found no evidence of erosive base on these F1G, and no gradation indicating transport by water current, thus F1G are interpreted as mass wasting deposits.

F1 is interbedded with a total number of 153 normally graded beds, characterized by a coarse sandy layer at the bottom to a progressively thinning upward silt size sequence. These layers are identified as facies F2. They are almost always associated to a thin white clay rich layer identified as Facies F3. Sometimes, the presence of pebbles was identified in the upper part of F2 and may either be related to the lamina deformation during coring, penetration of individual pebbles while deposited on unconsolidated sediment at the bottom of the lake or transported by a turbidity flow (Fig. 3). Due to their detrital-rich content and the fining upward trend (F2+F3) sequences represent high energy deposits interpreted as turbidites. The origin of each deposit is discussed in section 4.1.

Plotting the median grain size versus the coarsest and sorting parameter (Fig. 3c), highlights two distinct patterns. The normally graded beds (F2+F3) have a positive correlation of r=0.89 (n=315, p-value: <2.2e-16), and the mass wasting deposit layers have a correlation of r=0.90 (n=31, p-value: 9.24e-13) and higher Q90 values for an equivalent Q50. The differentiation between the two facies is particularly clear for high median values samples showing respectively higher Q90 and sorting values for the mass wasting deposits compared to turbidites. In contrast, F1A shows almost no grain size changes and thus has a low-energy depositional environment.

3.2.2. Correlation between seismic and sedimentary results

The base of the two units (Fig. 2 in red) and the strongest reflector, found respectively at 11.8, 17.3, 18.8 ms twtt correspond to 5.9, 8.6 and 15.3 m of sediment depth using an mean acoustic velocity of 1630 m.s^{-1}. Basal strong amplitude reflectors are indicative of strong acoustic impedance changes. Considering a change of grain size can be responsible of a change of reflectivity (Billeaud et al., 2005), the marked reflectors can indicate the presence of the coarse sediment layers. Moreover, both the undulated surface, potentially related to irregular thickness in sedimentary layers, as well as chaotic facies and the pinching out in a basinward direction, support the sedimentary interpretation of mass-wasting deposits. Given the depth

resolution of the seismic profile, theses three reflectors can be related to the three outstanding thick layers found in the sediment core at 6.35, 8.49 and 14.58 m.

3.3 CT scan based imagery

The CT scan methodology allowed the identification of 6433 individual mineralogical elements of at least 13 voxels (3.25 mm^3), corresponding to a minimum diameter of 2 mm. Total pebble repartition in the sediment core is described in terms of pebble counts per 5 mm interval (Fig. 4). We discarded the 2536 pebbles contained in the flood layers (F2+F3). At the end, 3897 pebbles were identified in the sediment facies F1G and interpreted as mass wasting deposits. The average volume of a particle was found to be 81 mm^3, corresponding to an average particle diameter of 4.3 mm. Based on these results, we identified 166 pebble-rich layers cumulating in at least 4 pebbles identified in 5 mm intervals. This limit of individuals within a deposit was found to be representative of historical avalanche records in the valley and exclude pebbles entering lake sediment related to slope processes such as natural chemical or mechanical weathering induced by frost and vegetation roots (Fouinat et al., 2017a).

3.4 Pollen record

The pollen diagram of Lake Lauvitel is expressed as percentages calculated from the total sum (Fig. 5). At 6.35 m, we identified a sharp vegetation change. From 15.45 m to 6.35 m, the majority of the pollen came from trees and shrubs, accounting for 65 to 90% of the pollen sum. The large representation of *Pinus*, *Abies*, and *Picea* in the tree pollen can be interpreted as the presence of a spruce forest in the watershed, probably a larger one than is there today. Current vegetation maps show the presence of such a forest but only at the southern part of the lake and associated with several isolated *Abies* and *Pinus cembra* trees in the western steep slopes. The palynological results suggest a more expansive forest than currently existed that probably also extended to the western watershed slopes. *Alnus* is present in 10 to 25% of the total pollen count, which is quite important proportion because they grow close to a source of water or in avalanche corridors. *Alnus* pollen, in this case, may be overrepresented due to the tributary transport. In addition, below 6.35 m, we found some evidence of *Rumex* and *Plantago*, providing evidence for a limited, but present grazing pressure, as well as traces of *Cerealia*. Overall, the pollen record provides evidence of the presence of human practices in the watershed, and these practices may have increased until a major vegetation change that is recorded 6.35 m depth in the sequence. Indeed, above this depth, the *Poaceae* proportion rapidly exceeds more than 50% of the pollen sum, and tree pollen, especially *Pinus*, *Picea* and *Abies*, exhibit a sharp decline. The decline of tree pollen coincides with an increase in the percentages of undetermined monoletes spores, and no change in *Polypodium* and *Pteridium*, which are also issued from ferns. From 6.35 m to the top of the sequence, we observe an increase in the anthropic taxa percentages. *Rumex* and *Plantago* were already present before and exhibit an increase, mirroring a rise in the grazing pressure, associated with the presence of *Cerealia* and *Juglans*, evidencing of crops and tree-gardening. Based on the pollen record, the maximum anthropic pressure is reached approximately at 4.58 m, when the *Juniperus* bushes reach a maximum, the *Picea* disappeared, and very low percentages of

Abies and *Pinus*. From 1.3 m to the top, pollen results show a progressive increase in trees probably expressing the continued decrease in land-use in this watershed.

3.5 Chronology

The recent sediment deposition study by Fouinat et al., (2017a) was based on short-lived radionuclides of which ^{210}Pb excess was calculated as the difference between total ^{210}Pb and ^{226}Ra activities. The low values of ^{210}Pb$_{ex}$ were excluded to reconstruct a synthetic sedimentary record following (Arnaud et al., 2002a). We obtained a mean accumulation rate of 3.7 +/- 0.3 mm yr^{-1} with age uncertainties derived from the standard error from the linear regression of the CFCS model (Goldberg, 1963). These low values of ^{210}Pb$_{ex}$ were attributed to flood deposits from the nearby Vénéon valley historical flood record from the RTM-ONF database (http://rtm-onf.ifn.fr/). In addition, a total of 19 radiocarbon analyses were performed on plant macroremains, twigs, leaves, tree bark and roots collected in the 15.44 m sediment sequence (Table 1). Among the results from the 19 samples, two dates were excluded from the age-depth model because they were considered too old, probably due to reworked material from the watershed. To develop a well-constrained chronology, we removed the 153 graded beds that were thicker than 5 mm and interpreted them as flood-induced deposits (Fouinat et al., 2017a) representing a total of 668.5 cm. The three mass wasting deposits exhibiting numerous pebble-sized elements, representing a total of 154 cm, were also excluded from the age-depth. The remaining 7.21 m (Fig. 6) were used to reconstruct a synthetic sedimentary record (Wilhelm et al., 2012a). The age-depth relationship was then calculated using a smooth spline interpolation generated using R software and the R-code package "Clam" version 2.2 (Blaauw, 2010).

4 Discussion

4.1 Event layers

4.1.1 Flood induced deposits

Normally graded beds identified by F2+F3 are common features in lake sediments where they are generally attributed to turbidity currents related to mass movements or flood deposits (Sturm and Matter, 1978; Arnaud et al., 2002b; Gilli et al., 2013). In the Q90-Q50 diagram (fig. 2c), the linear fit suggests an increase of coarser sediment transported and deposited with higher values of median, which was attributed to a sedimentary process regulated by water currents (Passega, 1964; Wilhelm et al., 2012b, 2015). The presence of terrestrial macroremains also suggests turbidity currents originating from the lake catchment. Within some of the turbidites the presence of pebbles was identified. The pebbles position within this deposit is quite random because they could be found in the coarse base as well as in the silty clay top of deposits. This feature does not suggest a transport of gravels with water current, especially as the main inlet is located at the southern part of the lake more than 300 meters from the coring site. However, a heavy rainfall triggering a flood would probably induce runoff in the steep slopes and avalanche corridors next to the coring site. The gravels within turbidites would likely be

originating from slopes processes above the coring site, supported by the angular shape and the size of >2-mm diameter related to short distance sediment transport. Moreover, the presence of coarse material identified by CT imagery can also be explained by in-core movement during coring.

4.1.2 Wet avalanche-induced deposits

We observed remarkable deposition of isolated (F1A) as well as aggregated pebbles (F1G) within the fine sediment matrix. Based on the Q90-Q50 diagram (fig. 2c) similar median values are characterizing F1A and F1G facies suggesting similar deposition energy. However, both Q90 and sorting values are higher for F1G which is related to an additional sandy fraction in the fine sediment, inducing multi-modal grain size distribution (Fouinat et al., 2017a). As observed on pebbles present in the flood-induced deposits, both the angular shape and the large size suggest short-distance transport. Moreover, based on the grain size measurements we didn't identify evidence of gradation or erosive base characterizing debris flow in lacustrine environment, thus excluding a dense subaqueous sediment transport (Sletten et al., 2003; Irmler et al., 2006). The coarse material would then be transported from the steep slopes, without water current and deposited in the lake basin. Observations in the western part of the watershed, of both wet avalanches cones at the bottom of the avalanche corridors, suggest pebbles origin from the steep slopes. Due to their density and high water content, wet avalanches occurring preferably in spring season, would be either deposited on the lake ice or directly in the water if the ice was already melted. The transported coarse sediment fraction would in the first case be stored on lake ice, and then be spread to the lake basin by drifting ice and deposited as drop stones at spring season (Luckman, 1975; Nesje et al., 2007; Vasskog et al., 2011). This scenario would also depend on the quantity of sediment transported and the magnitude of the avalanche flow. From our results it seems difficult to estimate an avalanche magnitude which would probably depend on the quantity of material transported and the distance from the avalanche corridor. In this case, a multi-coring study would be more appropriate to precisely characterize the spread of those avalanche deposits. However, a high magnitude avalanche would probably break the ice and sediment would enter directly into water, creating a large aggregation of sediment at the bottom. This is more likely the case for the three thicker mass-wasting deposits found in LAU11 characterized by heterogeneous fine sediment fractions, numerous pebbles (fig. 3) and beveled units in the seismic profiles (Fig. 2).

4.2 Potential influence of vegetation on the avalanche and flood chronicles

To understand the potential impacts of past human landscape management on the flood and avalanche chronicles, we investigated the past vegetation dynamics. From 3300 to 760 yrs cal. BP, pollen analysis exhibits fluctuations of the arboreal taxa from 55% to 90% of the total pollen counts, with lower arboreal pollen percentages coinciding with higher percentages of the anthropic taxa (Fig. 7). Those anthropogenic pollens were identified as *Plantago and Rumex*, suggesting the occurrence of grazing activities, and as *Cerealia*, suggesting the presence of crops. Approximately 760 yrs cal. BP (+/- 50), a

major shift in the vegetation cover is interpreted from a drop of the *Pinus* taxa counts and other trees such as *Abies*, *Pinus*, *Picea* as well as a sharp increase in *Poaceae* based on the herb pollen sum nearly reaching 50% of the total pollen counts. The increase in the herb group coincides with a clear increase in undetermined monoletes spores related to ferns present in the undergrowth taxa. However, at the same time, we do not observe any increase in the *Polypodium* or *Pteridium* ferns taxa.

5   The presence of the monoletes spores could then be related to the reworking of litter material by the erosion of the old spores due to tree clearance (Fig. 5). The pollen record exhibits a progressive increase in the anthropic taxa, leading to a major vegetation change probably related to a strong human pressure. This hypothesis is supported by nearby pollen records exhibiting an increase in the anthropic taxa at comparable dates (Coûteaux, 1983; Tessier et al., 1993; Nakagawa et al., 2000). In the same period, the avalanche record exhibits a considerable increase in frequency (Fig.7). In addition, we observe

10   the last thick (52 cm) avalanche event of the entire chronicle, dated at 760 yrs cal. BP, denoting poor stabilization of the sediment on the slopes during this period. Based on the pollen analysis and avalanche characteristics, we interpret this event as a result of a major vegetation change related to human practices. Supporting this hypothesis, the average number of avalanches recorded before the deforestation is 2.2 per century, and after 780 yrs cal. BP, increases to 13.3 per century, increasing the probability to record a wet avalanche by a factor of six. We consider this deforestation to be the trigger of a

15   major tipping point in the avalanche regimes. In the case of Lake Lauvitel, the avalanche recurrence strongly increased with the human-induced land cover changes, especially in the western part of the watershed hosting the avalanche corridors. Similar observations led García-Hernández et al., (2017) to attribute observed avalanche frequency rise to an increasing in grazing pressure in the Asturian Massif (NW of Spain) at the end of the 19th century. The reconstructed flood frequency increase coincides with the presence of anthropic taxa in the pollen diagram, even before the land opening event. Moreover,

20   higher flood frequency is also observed when *Pinus* pollen is found in lower proportions 2380-1930, 1430-1360, 1110-970, 640-520 yrs cal. BP, and additionally after the land opening event at 780 yrs cal. BP. Human activities influencing vegetation dynamics in the southern part of the watershed is also supported by the presence of micro-charcoal found in soils. Human activities in those type of alpine lake settings can have a significant impact on flood activity as previously suggested (Giguet-Covex et al., 2011; Brisset et al., 2017). Erosion processes modalities in the southern part of the catchment are still

25   to be studied in order to establish a reliable sediment-based flood chronicle for Lake Lauvitel.

4.3 Climate forcing on wet avalanches

4.3.1 Wet avalanche occurrence compared to climatic instrumental data over the last 350 years

The presence of pebbles (>2 mm) in Lake Lauvitel sediment, identified through numerical counting, allows us to reconstruct past avalanche activity (Fouinat et al., 2017a). Wet avalanches are generally interpreted as being triggered by snowpack

30   destabilization mainly due to both thick snow cover and high spring temperature. To assess the local reliability, we compared spring temperature (AMJ) (Fig. 8b) and winter precipitation (DJFMA) (Fig. 8c) since AD 1660 based on instrumental record

and documentary proxy data on a monthly basis from Casty et al., (2005). Data is geographically centered on the study site on a 0.5°x0.5° spatial grid and averaged over a 31-year period in order to avoid inter-annual variability.

During the last 350 years, we distinguish between two main intervals T1 and T2 (AD 1660-1840 and 1840-2000) based on a transition between the minimum arboreal pollen proportions (T1: 45%) to a progressive increase to values similar to before the tipping point (T2: 80%). Given vegetation has an effect on avalanche occurrence; we need to compare climatic setting within each main interval potentially influencing higher avalanche frequency (grey bands, P2: AD 1720-1840, P4: AD 1920-1940, P6: AD 1969-1992). Within T1, 97% of avalanches occur during the period P2, which is characterized by warmer median, third quartile and extreme values of spring temperature. Winter precipitations are exhibiting higher extreme values but lower median and third quartile probably denoting a thinner snow cover than P1. According to climate parameters, during low arboreal pollen proportion, avalanches occur preferably during periods of warmer spring temperatures but with relatively less winter precipitations. Warmer temperatures enhance snow melting and increase probabilities to have a rain on snow event, favorable to wet avalanches occurrence (Baggi and Schweizer, 2009; Eckert et al., 2013).

In the T2 interval, higher avalanche frequency periods (P4 and P6) exhibit the lowest spring temperatures median and extreme values. In addition, winter precipitations are notably higher (median values, third quartile and extreme values). Thus, avalanches occur preferably during periods of extreme winter precipitations, rather than periods of warmer spring temperature. Based on increased tree cover, more frequent avalanche occurrence could be related to either increased snow loading at lower altitudes or destabilization of the thick snowpack at higher altitudes (e.g. beyond tree line) later in the season.

The longest avalanche record of the French Alps is based on tree rings along the Echalp avalanche path (Fig. 8a), situated approximately 70 km southeast of Lake Lauvitel in the Queyras massif (Corona et al., 2013). Two periods with high avalanche activity have been identified as AD 1802-1820, 1846-1867. Considering our age model uncertainties at this period (+/- 48 yrs cal. BP), these two periods could correspond to the two avalanche frequency peaks in Lake Lauvitel (AD 1760-1780, 1800-1820). Moreover, period AD 1970-1980, known for heavy snow fall in the Alps (Castebrunet et al., 2012), exhibit events in both records. A perfect concordance between those two records is however unlikely as avalanches are controlled by specific extreme weather conditions. Reardon et al., (2008) found that environmental parameters such as vegetation cover are influencing avalanche triggers and that the occurrence of avalanches is associated with positive snowpack anomalies. As snow loading depends on wind direction, discrepancies in snow accumulation are possible from one valley to another (McCollister et al., 2003). In the end, the Lake Lauvitel pebble deposits are in accordance with climate parameters and seem representative of at least the valley sensitivity to avalanches.

4.3.2 Past wet avalanche activity under regional climatic setting

To investigate the 3300 years-long wet avalanche chronicle (Fig. 9), we compare our avalanche chronicle with records related to winter precipitation and temperature over several millennia. It is commonly accepted that the major factors forcing the Alpine glacial extent are annual temperature and winter precipitation (Vincent, 2005; Solomina et al., 2016). The Mer de

Glace glacier length record (Le Roy et al., 2015), located in the western French Alps, as well as the proglacial Lake Muzelle record, located 3 km from the study site (Fouinat et al., 2017b), allow long-term comparison with past glacier dynamics. Additionally, temperature variability is issued from the central European relative summer temperature reconstruction from Büntgen et al. (2011) based on pine and larch tree-rings at high altitude in the alpine region.

5   Lake Lauvitel higher wet avalanche frequency occurred at 2570-2510, 2250-2180, 2090-2050, 1945-1910, 1660-1570, 1460-1320, 860-1730, 640-440, 370-290, 250-90 yrs cal. BP (in grey, fig. 9d) which coincides with periods of larger extent of the Mer de Glace glacier (Fig. 9c). The only exception is dated at 2250-1910 yrs cal. BP, when high frequency is coinciding with a retreated phase of the Mer de Glace, but is synchronous with a local glacier advance in the Ecrins massif (Le Roy et al., 2017), as well as enhanced glacial activity issued from Lake Bramant sediment record (Guyard et al., 2007). It is

10   probable, for wet avalanches to occur on a multi-centennial time scale, that sufficient winter precipitations are necessary to produce a thick enough snow cover. This result is supported by previous studies on avalanche deposits recorded in lake sediment which attributed increased occurrence to the climate-driven increase in glacial activity (Blikra and Nemec, 1998; Nesje et al., 2007). However, at a sub-centennial scale, Lake Lauvitel avalanches frequency peaks also coincide with both periods of lower clastic input in nearby proglacial Lake Muzelle denoting a lower influence of glacier erosion in lake

15   sediment (fig. 9b), and with warmer relative European summer temperatures (fig. 9a). In this case, temperature control on avalanche occurrence could be significant and would affect the snow cover and create more frequent wet avalanches.

Over long periods, our study highlights both the role of climate parameters (temperature and winter precipitation) and vegetation cover changes on the past wet avalanche hazard. The role of increased winter precipitations related to large glacier advances, is essential on snow pack thickness for avalanches to occur. Within these periods, the thick snow pack

20   seems to be preferably destabilised by warmer spring temperatures. In the context of predicted warmer temperatures, wet avalanches could be more frequent, especially in low-forested areas or higher altitudes, either induced by warmer spring temperatures or rain on snow. Further long-term wet avalanches records in the alpine area would help to better understand special extent of these forcing parameters and verify our interpretations.

5 Conclusion

25   High resolution sedimentological and CT imagery analyses of Lake Lauvitel sequence revealed 319 event layers over the last 3300 years. 153 of these deposits present a fining upward trend with a strong relationship between median values and coarser percentile suggesting a water current origin. These events were interpreted as flood related deposits. The other 166 deposits were characterized by a multimodal grain size distribution with presence of a sand fraction but also gravel and pebble size minerogenic elements within a fine sediment matrix with no evidence of gradation. They were interpreted as induced by wet

30   avalanches. Local human activity was reconstructed using pollen analysis, and revealed a major vegetation change at 780 yrs cal. BP (+/- 50 yrs) interpreted as a large forest clearance. This period may have induced a shift in wet avalanche occurrence and may have caused a tipping point significantly increasing their frequency after this human induced landscape change.

The comparison between instrumental and climate records on a multi-centennial scale shows that wet avalanches in Lake Lauvitel preferably occur during larger glacial extent when climate conditions induce a sufficiently thick snow cover. On a sub-centennial timescale, events are more frequent when spring temperature is warmer, generating snow pack destabilization and/or an increase of rain on snow. Higher winter precipitations have the same effect, even while spring temperatures are relatively colder denoting a probable snow pack destabilization later in the season. Thus, the combination of high winter precipitation and warmer temperatures seem to be major climatic forcing on the occurrence of wet avalanches in Lake Lauvitel both under low and high anthropic pressure on the watershed. In the Alps, predicted warmer temperatures may induce an evolution of the avalanche hazard towards more wet avalanches especially at higher altitudes. Further studies on wet avalanches are necessary in order to better understand past occurrence and climate forcing of these events on a regional scale.

Author contribution

Laurent Fouinat, Pierre Sabatier, Jérôme Poulenard, Fabien Arnaud have elaborated the manuscript with contributions from all co-authors. Fernand David was in charge of the pollen record. Xavier Montet has made the CT scan measurements, Eric Chaumillon performed the seismic campaign and Philippe Schoeneich is the leader of the project.

Competing interests

The authors declare that they have no conflict of interest.

Acknowledgements

Laurent Fouinat's PhD fellowship was supported by a grant from Ecrins National Park, Communauté des Communes de l'Oisans, Deux Alpes Loisirs and the Association Nationale de la Recherche et de la Technologie (ANRT). The coring campaign was funded by a grant of the Pole Grenoblois Risques Naturels. Authors would like to thank the Ecrins National Park (PNE) for the coring authorization and assistance on the field. Thank you to CLIM-COR Continent for coring facilities.[14]C analyses were acquired thanks to the CNRS-INSU ARTEMIS national radiocarbon AMS measurement programme at Laboratoire de Mesure 14C (LMC14) in the CEA Institute at Saclay (French Atomic Energy Commission), and the Poznan Radiocarbon Laboratory. The Authors wish to thank the Hôpitaux Univeritaire de Genève (HUG) for the CT scan measurements.

References

Ancey, C., Bain, V., 2015. Dynamics of glide avalanches and snow gliding: Glide avlanches and snow gliding. Reviews of Geophysics 53, 745–784. https://doi.org/10.1002/2015RG000491

Arnaud, F., Lignier, V., Revel, M., Desmet, M., Beck, C., Pourchet, M., Charlet, F., Trentesaux, A., Tribovillard, N., 2002a. Flood and earthquake disturbance of 210Pb geochronology (Lake Anterne, NW Alps). Terra Nova 14, 225–232.

Arnaud, F., Lignier, V., Revel, M., Desmet, M., Beck, C., Pourchet, M., Charlet, F., Trentesaux, A., Tribovillard, N., 2002b. Flood and earthquake disturbance of 210Pb geochronology (Lake Anterne, NW Alps). Terra Nova 14, 225–232.

5   Baggi, S., Schweizer, J., 2009. Characteristics of wet-snow avalanche activity: 20 years of observations from a high alpine valley (Dischma, Switzerland). Natural Hazards 50, 97–108.

Billeaud, I., Chaumillon, E., Weber, O., 2005. Evidence of a major environmental change recorded in a macrotidal bay (Marennes-Oléron Bay, France) by correlation between VHR seismic profiles and cores. Geo-Marine Letters 25, 1–10.

10 Blaauw, M., 2010. Methods and code for 'classical' age-modelling of radiocarbon sequences. Quaternary Geochronology 5, 512–518. https://doi.org/10.1016/j.quageo.2010.01.002

Blikra, Nemec, 1998. Postglacial colluvium in western Norway: depositional processes, facies and palaeoclimatic record. Sedimentology 45, 909–959. https://doi.org/10.1046/j.1365-3091.1998.00200.x

Bøe, A.-G., Dahl, S.O., Lie, Ø., Nesje, A., 2006. Holocene river floods in the upper Glomma catchment, southern Norway: a
15 high-resolution multiproxy record from lacustrine sediments. The Holocene 16, 445–455.

Bolte, S., Cordelieres, F.P., 2006. A guided tour into subcellular colocalization analysis in light microscopy. Journal of microscopy 224, 213–232.

Brisset, E., Guiter, F., Miramont, C., Troussier, T., Sabatier, P., Poher, Y., Cartier, R., Arnaud, F., Malet, E., Anthony, E.J.,
2017. The overlooked human influence in historic and prehistoric floods in the European Alps. Geology 45, 347–
20 350. https://doi.org/10.1130/G38498.1

Büntgen, U., Tegel, W., Nicolussi, K., McCormick, M., Frank, D., Trouet, V., Kaplan, J.O., Herzig, F., Heussner, K.-U., Wanner, H., Luterbacher, J., Esper, J., 2011. 2500 Years of European Climate Variability and Human Susceptibility. Science 331, 578–582. https://doi.org/10.1126/science.1197175

Buntgen, U., Tegel, W., Nicolussi, K., McCormick, M., Frank, D., Trouet, V., Kaplan, J.O., Herzig, F., Heussner, K.-U.,
25 Wanner, H., Luterbacher, J., Esper, J., 2011. 2500 Years of European Climate Variability and Human Susceptibility. Science 331, 578–582. https://doi.org/10.1126/science.1197175

Castebrunet, H., Eckert, N., Giraud, G., 2012. Snow and weather climatic control on snow avalanche occurrence fluctuations over 50 yr in the French Alps. Climate of the Past 8, p–855.

Castebrunet, H., Eckert, N., Giraud, G., Durand, Y., Morin, S., 2014. Projected changes of snow conditions and avalanche
30 activity in a warming climate: the French Alps over the 2020-2050 and 2070-2100 periods. Cryosphere 8, 1673–1697.

Casty, C., Wanner, H., Luterbacher, J., Esper, J., Böhm, R., 2005. Temperature and precipitation variability in the European Alps since 1500. International Journal of Climatology 25, 1855–1880. https://doi.org/10.1002/joc.1216

Corona, C., Georges, R., Jérôme, L.S., Markus, S., Pascal, P., 2010. Spatio-temporal reconstruction of snow avalanche
35 activity using tree rings: Pierres Jean Jeanne avalanche talus, Massif de l'Oisans, France. CATENA 83, 107–118. https://doi.org/10.1016/j.catena.2010.08.004

Corona, C., Saez, J.L., Stoffel, M., Rovera, G., Edouard, J.-L., Berger, F., 2013. Seven centuries of avalanche activity at Echalp (Queyras massif, southern French Alps) as inferred from tree rings. The Holocene 23, 292–304. https://doi.org/10.1177/0959683612460784

40 Coûteaux, M., 1983. Fluctuations glaciaires de la fin du Würm dans les Alpes françaises, établies par des analyses polliniques. Boreas 12, 35–56.

Delunel, R., Hantz, D., Braucher, R., Bourlès, D.L., Schoeneich, P., Deparis, J., 2010. Surface exposure dating and geophysical prospecting of the Holocene Lauvitel rock slide (French Alps). Landslides 7, 393–400. https://doi.org/10.1007/s10346-010-0221-0

45 Eckert, N., Keylock, C.J., Castebrunet, H., Lavigne, A., Naaim, M., 2013. Temporal trends in avalanche activity in the French Alps and subregions: from occurrences and runout altitudes to unsteady return periods. Journal of Glaciology 59, 93–114. https://doi.org/10.3189/2013JoG12J091

Faegri, K., Kaland, P.E., Krzywinski, K., 1989. Textbook of pollen analysis. John Wiley & Sons Ltd.

Fierz, C., Armstrong, R.L., Durand, Y., Etchevers, P., Greene, E., McClung, D.M., Nishimura, K., Satyawali, P.K.,
50 Sokratov, S.A., 2009. The international classification for seasonal snow on the ground. UNESCO/IHP Paris.

Fouinat, L., Sabatier, P., Poulenard, J., Reyss, J.-L., Montet, X., Arnaud, F., 2017a. A new CT scan methodology to characterize a small aggregation gravel clast contained in a soft sediment matrix. Earth Surface Dynamics 5, 199–209. https://doi.org/10.5194/esurf-5-199-2017

Fouinat, L., Sabatier, P., Poulenard, J., Etienne, D., Crouzet, C., Develle, A.-L., Doyen, E., Malet, E., Reyss, J.-L., Sagot, C., Bonet, R., Arnaud, F., 2017b. One thousand seven hundred years of interaction between glacial activity and flood frequency in proglacial Lake Muzelle (western French Alps). Quaternary Research 87, 407–422. https://doi.org/10.1017/qua.2017.18

García-Hernández, C., Ruiz-Fernández, J., Sánchez-Posada, C., Pereira, S., Oliva, M., Vieira, G., 2017. Reforestation and land use change as drivers for a decrease of avalanche damage in mid-latitude mountains (NW Spain). Global and Planetary Change 153, 35–50. https://doi.org/10.1016/j.gloplacha.2017.05.001

Giguet-Covex, C., Arnaud, F., Enters, D., Poulenard, J., Millet, L., Francus, P., David, F., Rey, P.-J., Wilhelm, B., Delannoy, J.-J., 2012. Frequency and intensity of high-altitude floods over the last 3.5ka in northwestern French Alps (Lake Anterne). Quaternary Research 77, 12–22. https://doi.org/10.1016/j.yqres.2011.11.003

Giguet-Covex, C., Arnaud, F., Poulenard, J., Disnar, J.-R., Delhon, C., Francus, P., David, F., Enters, D., Rey, P.-J., Delannoy, J.-J., 2011. Changes in erosion patterns during the Holocene in a currently treeless subalpine catchment inferred from lake sediment geochemistry (Lake Anterne, 2063 m a.s.l., NW French Alps): The role of climate and human activities. The Holocene 21, 651–665. https://doi.org/10.1177/0959683610391320

Gilli, A., Anselmetti, F.S., Glur, L., Wirth, S.B., 2013. Lake sediments as archives of recurrence rates and intensities of past flood events, in: Dating Torrential Processes on Fans and Cones. Springer, pp. 225–242.

Goeury, C., 1988. Acquisition, gestion et représentation des données de l'analyse pollinique sur micro-ordinateur. Travaux de la section scientifique et technique. Institut français de Pondichéry 25, 405–416.

Goldberg, E.D., 1963. Geochronology with 210Pb. Radioactive dating 121–131.

Guyard, H., Chapron, E., St-Onge, G., Anselmetti, F.S., Arnaud, F., Magand, O., Francus, P., Mélières, M.-A., 2007. High-altitude varve records of abrupt environmental changes and mining activity over the last 4000 years in the Western French Alps (Lake Bramant, Grandes Rousses Massif). Quaternary Science Reviews 26, 2644–2660. https://doi.org/10.1016/j.quascirev.2007.07.007

Irmler, R., Daut, G., Mäusbacher, R., 2006. A debris flow calendar derived from sediments of lake Lago di Braies (N. Italy). Geomorphology 77, 69–78. https://doi.org/10.1016/j.geomorph.2006.01.013

Iverson, R.M., 1997. The physics of debris flows. Reviews of geophysics 35, 245–296.

Lazar, B., Williams, M., 2008. Climate change in western ski areas: Potential changes in the timing of wet avalanches and snow quality for the Aspen ski area in the years 2030 and 2100. Cold regions science and technology 51, 219–228.

Le Roy, M., Deline, P., Carcaillet, J., Schimmelpfennig, I., Ermini, M., 2017. 10Be exposure dating of the timing of Neoglacial glacier advances in the Ecrins-Pelvoux massif, southern French Alps. Quaternary Science Reviews 178, 118–138. https://doi.org/10.1016/j.quascirev.2017.10.010

Le Roy, M., Nicolussi, K., Deline, P., Astrade, L., Edouard, J.-L., Miramont, C., Arnaud, F., 2015. Calendar-dated glacier variations in the western European Alps during the Neoglacial: the Mer de Glace record, Mont Blanc massif. Quaternary Science Reviews 108, 1–22. https://doi.org/10.1016/j.quascirev.2014.10.033

Luckman, B., 1975. Drop stones resulting from snow-avalanche deposition on lake ice. Journal of Glaciology 14, 186–188.

Luckman, B., 1977. The geomorphic activity of snow avalanches. Geografiska Annaler. Series A. Physical Geography 31–48.

Martin, J.-P., Germain, D., 2016. Can we discriminate snow avalanches from other disturbances using the spatial patterns of tree-ring response? Case studies from the Presidential Range, White Mountains, New Hampshire, United States. Dendrochronologia 37, 17–32. https://doi.org/10.1016/j.dendro.2015.12.004

McCollister, C., Birkeland, K., Hansen, K., Aspinall, R., Comey, R., 2003. Exploring multi-scale spatial patterns in historical avalanche data, Jackson Hole Mountain Resort, Wyoming. Cold Regions Science and Technology 37, 299–313.

Moore, J.R., Egloff, J., Nagelisen, J., Hunziker, M., Aerne, U., Christen, M., 2013. Sediment Transport and Bedrock Erosion by Wet Snow Avalanches in the Guggigraben, Matter Valley, Switzerland. Arctic, Antarctic, and Alpine Research 45, 350–362. https://doi.org/10.1657/1938-4246-45.3.350

Mulder, T., Migeon, S., Savoye, B., Faugères, J.-C., 2001. Inversely graded turbidite sequences in the deep Mediterranean: a record of deposits from flood-generated turbidity currents? Geo-Marine Letters 21, 86–93. https://doi.org/10.1007/s003670100071

Nakagawa, T., Edouard, J.-L., de Beaulieu, J.-L., 2000. A scanning electron microscopy (SEM) study of sediments from Lake Cristol, southern French Alps, with special reference to the identification of Pinus cembra and other Alpine Pinus species based on SEM pollen morphology. Review of Palaeobotany and Palynology 108, 1–15. https://doi.org/10.1016/S0034-6667(99)00030-5

Nesje, A., Bakke, J., Dahl, S.O., Lie, O., Boe, A.-G., 2007. A continuous, high-resolution 8500-yr snow-avalanche record from western Norway. The Holocene 17, 269–277. https://doi.org/10.1177/0959683607075855

Passega, R., 1964. Grain size representation by CM patterns as a geological tool. Journal of Sedimentary Research 34, 830–847.

Reardon, B., Pederson, G., Caruso, C., Fagre, D., 2008. Spatial reconstructions and comparisons of historic snow avalanche frequency and extent using tree rings in Glacier National Park, Montana, USA. Arctic, Antarctic, and Alpine Research 40, 148–160.

Reimer, P.J., Bard, E., Bayliss, A., Beck, J.W., Blackwell, P.G., Ramsey, C.B., Buck, C.E., Cheng, H., Edwards, R.L., Friedrich, M., 2013. IntCal13 and Marine13 radiocarbon age calibration curves 0–50,000 years cal BP. Radiocarbon 55, 1869–1887.

Schindelin, J., Arganda-Carreras, I., Frise, E., Kaynig, V., Longair, M., Pietzsch, T., Preibisch, S., Rueden, C., Saalfeld, S., Schmid, B., 2012. Fiji: an open-source platform for biological-image analysis. Nature methods 9, 676–682.

Sletten, K., Blikra, L.H., Ballantyne, C., Nesje, A., Dahl, S.O., 2003. Holocene debris flows recognized in a lacustrine sedimentary succession: sedimentology, chronostratigraphy and cause of triggering. The Holocene 13, 907–920.

Solomina, O.N., Bradley, R.S., Jomelli, V., Geirsdottir, A., Kaufman, D.S., Koch, J., McKay, N.P., Masiokas, M., Miller, G., Nesje, A., Nicolussi, K., Owen, L.A., Putnam, A.E., Wanner, H., Wiles, G., Yang, B., 2016. Glacier fluctuations during the past 2000 years. Quaternary Science Reviews 149, 61–90. https://doi.org/10.1016/j.quascirev.2016.04.008

Stoffel, M., Bollschweiler, M., 2008. Tree-ring analysis in natural hazards research – an overview. Nat. Hazards Earth Syst. Sci. 8, 187–202. https://doi.org/10.5194/nhess-8-187-2008

Sturm, M., Matter, A., 1978. Turbidites and Varves in Lake Brienz (Switzerland): Deposition of Clastic Detritus by Density Currents, in: Modern and Ancient Lake Sediments. Blackwell Publishing Ltd., pp. 147–168.

Tessier, L., Beaulieu, J.-L.D., Couteaux, M., Edouard, J.-L., Ponel, P., Rolando, C., Thinon, M., Thomas, A., Tobolski, K., 1993. Holocene palaeoenvironments at the timberline in the French Alps—a multidisciplinary approach. Boreas 22, 244–254. https://doi.org/10.1111/j.1502-3885.1993.tb00184.x

Touflan, P., Talon, B., Walsh, K., 2010. Soil charcoal analysis: a reliable tool for spatially precise studies of past forest dynamics: a case study in the French southern Alps. The Holocene 20, 45–52. https://doi.org/10.1177/0959683609348900

Valt, M., Paola, C., 2013. Climate change in Italian Alps: Analysis of snow precipitation, snow durations and avalanche activity. Presented at the International Snow Science Workshop, pp. 1247–1250.

Vasskog, K., Nesje, A., Storen, E.N., Waldmann, N., Chapron, E., Ariztegui, D., 2011. A Holocene record of snow-avalanche and flood activity reconstructed from a lacustrine sedimentary sequence in Oldevatnet, western Norway. The Holocene 21, 597–614. https://doi.org/10.1177/0959683610391316

Vincent, C., 2005. Solving the paradox of the end of the Little Ice Age in the Alps. Geophysical Research Letters 32, 9706. https://doi.org/10.1029/2005GL022552

Wilhelm, B., Arnaud, F., Enters, D., Allignol, F., Legaz, A., Magand, O., Revillon, S., Giguet-Covex, C., Malet, E., 2012a. Does global warming favour the occurrence of extreme floods in European Alps? First evidences from a NW Alps proglacial lake sediment record. Climatic Change 113, 563–581. https://doi.org/10.1007/s10584-011-0376-2

Wilhelm, B., Arnaud, F., Sabatier, P., Crouzet, C., Brisset, E., Chaumillon, E., Disnar, J.-R., Guiter, F., Malet, E., Reyss, J.-L., Tachikawa, K., Bard, E., Delannoy, J.-J., 2012b. 1400years of extreme precipitation patterns over the Mediterranean French Alps and possible forcing mechanisms. Quaternary Research 78, 1–12. https://doi.org/10.1016/j.yqres.2012.03.003

Wilhelm, B., Sabatier, P., Arnaud, F., 2015. Is a regional flood signal reproducible from lake sediments? Sedimentology 62, 1103–1117. https://doi.org/10.1111/sed.12180
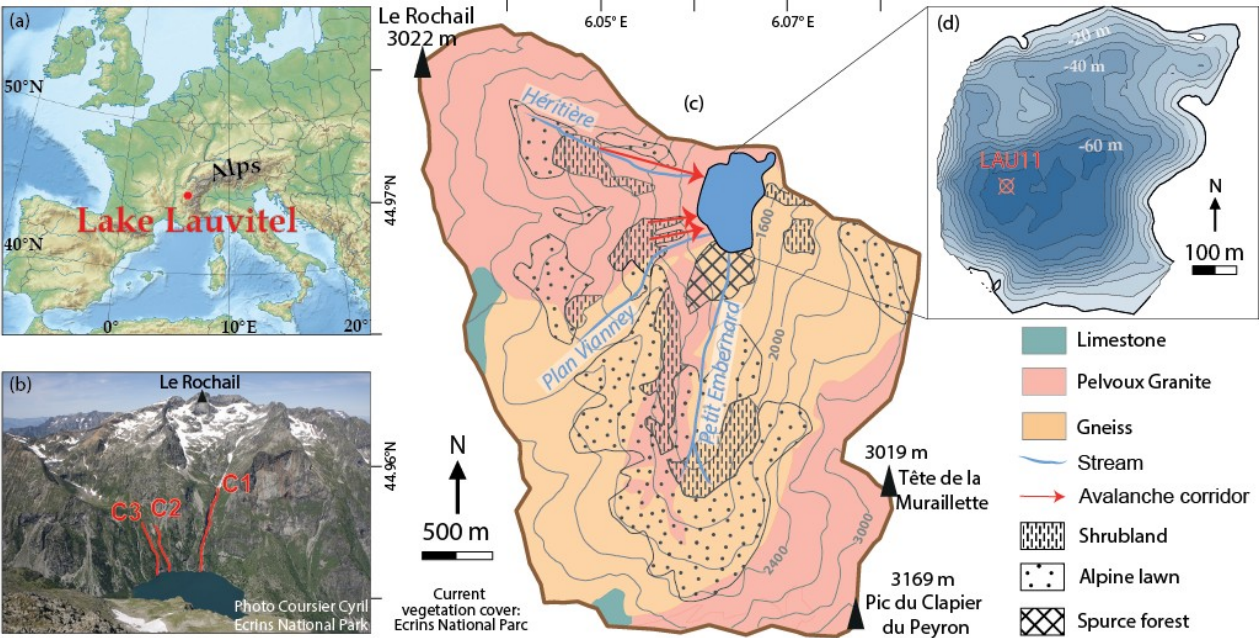
Figure 1: a) Location of Lake Lauvitel in the western Alps. b) Photograph towards the west of the lake watershed exhibiting three avalanche corridors. c) Simplified geological maps of Lake Lauvitel watershed and current vegetation cover. d) Lake bathymetry and position of LAU11 sediment core.
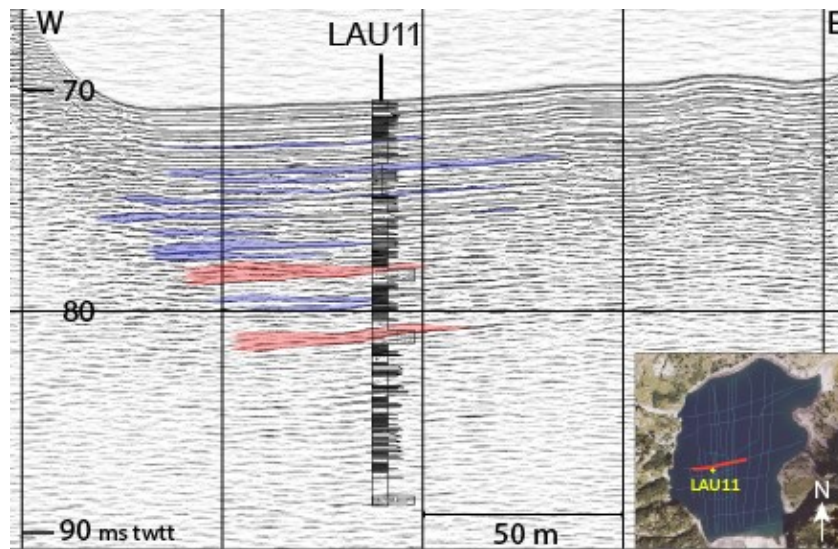
Figure 2: Interpreted seismic profile 03_6 on a W-E direction. LAU11 coring point is indicated by the vertical bar and the simplified core results. Red units are interpreted as mass wasting deposits and thinner blue layers are interpreted as containing coarse sediments.
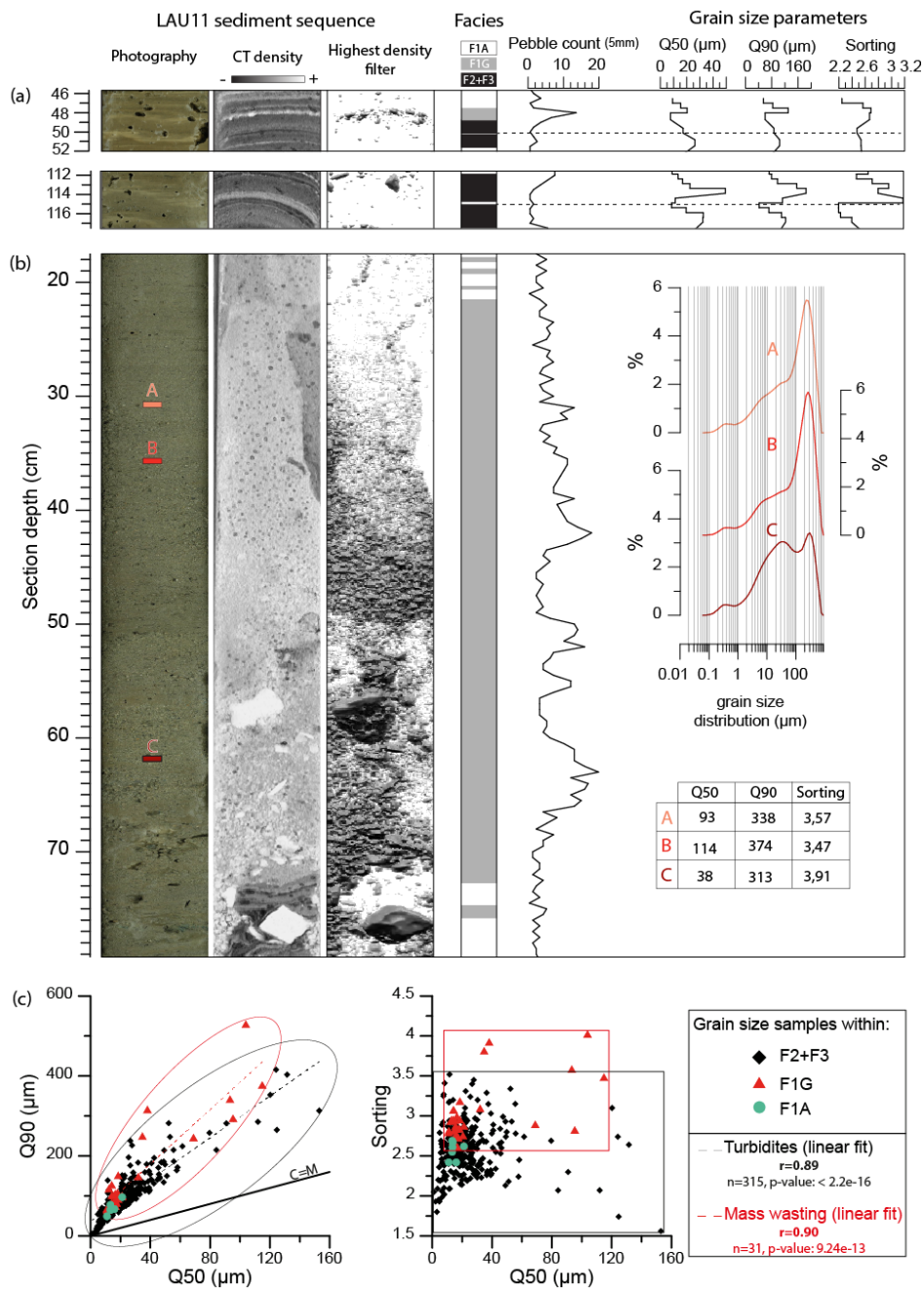
Figure 3: LAU11 core photography compared with CT scan radiograph and high density filter in function of depth. Images are plotted versus grain size parameters and the pebble counts as a sum in a 5 mm depth. (a) Typical facies found in Lauvitel sediment sequence (b) Outstanding F1G 52 cm thick layer identified at 6.86 m in the sequence (c) Bi-plots exhibiting median (Q50) versus coarser percentile (Q90) and sorting parameter of LAU11 grain size measurements in function of deposits types.
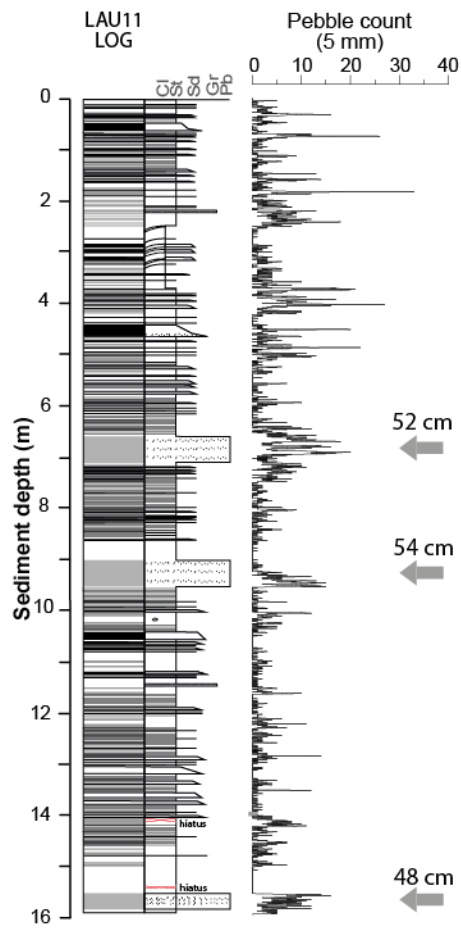
Figure 4: LAU11 sediment sequence Log versus the total pebbles counts in function of depth. On the right, each of the three outstanding F1G deposits thickness identified at depths 6.35, 8.49 and 14.58 meters.
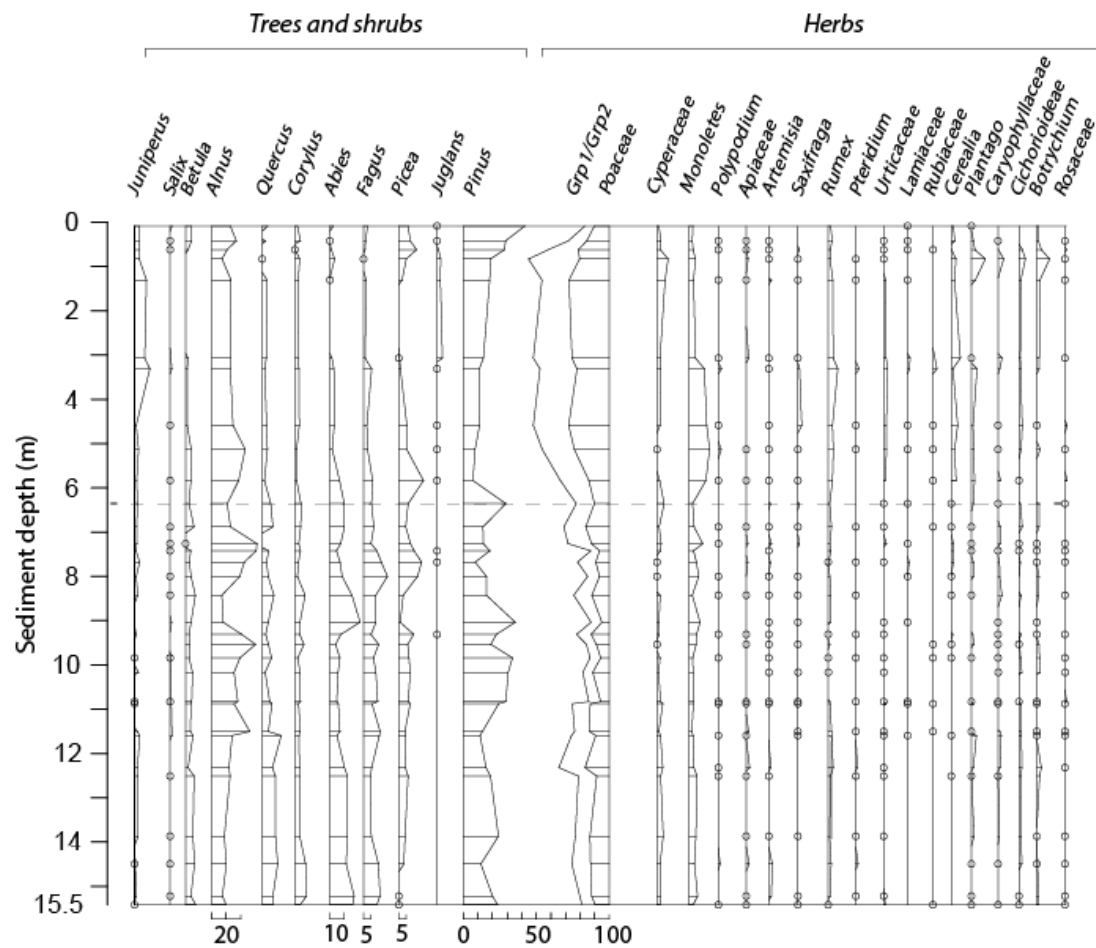
Figure 5. Simplified pollen of LAU11 sediment sequence in function of depth as a percentage of the pollen sum. Dashed line refers to depth 6.35 m. Dots refer to values below 1% of the pollen sum.
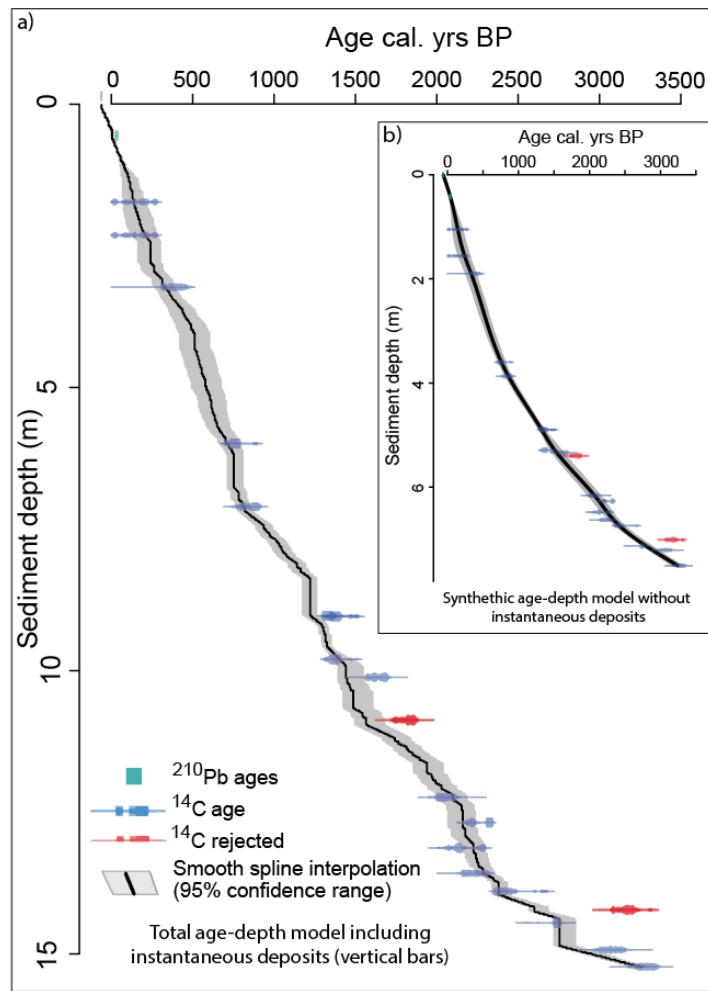
Figure 6: a) Age-depth model for entire LAU11 sediment sequence including instantaneous deposits based on short-lived radionuclides and radiocarbon derived ages. b) Synthethic age-depth model free of events for LAU11.
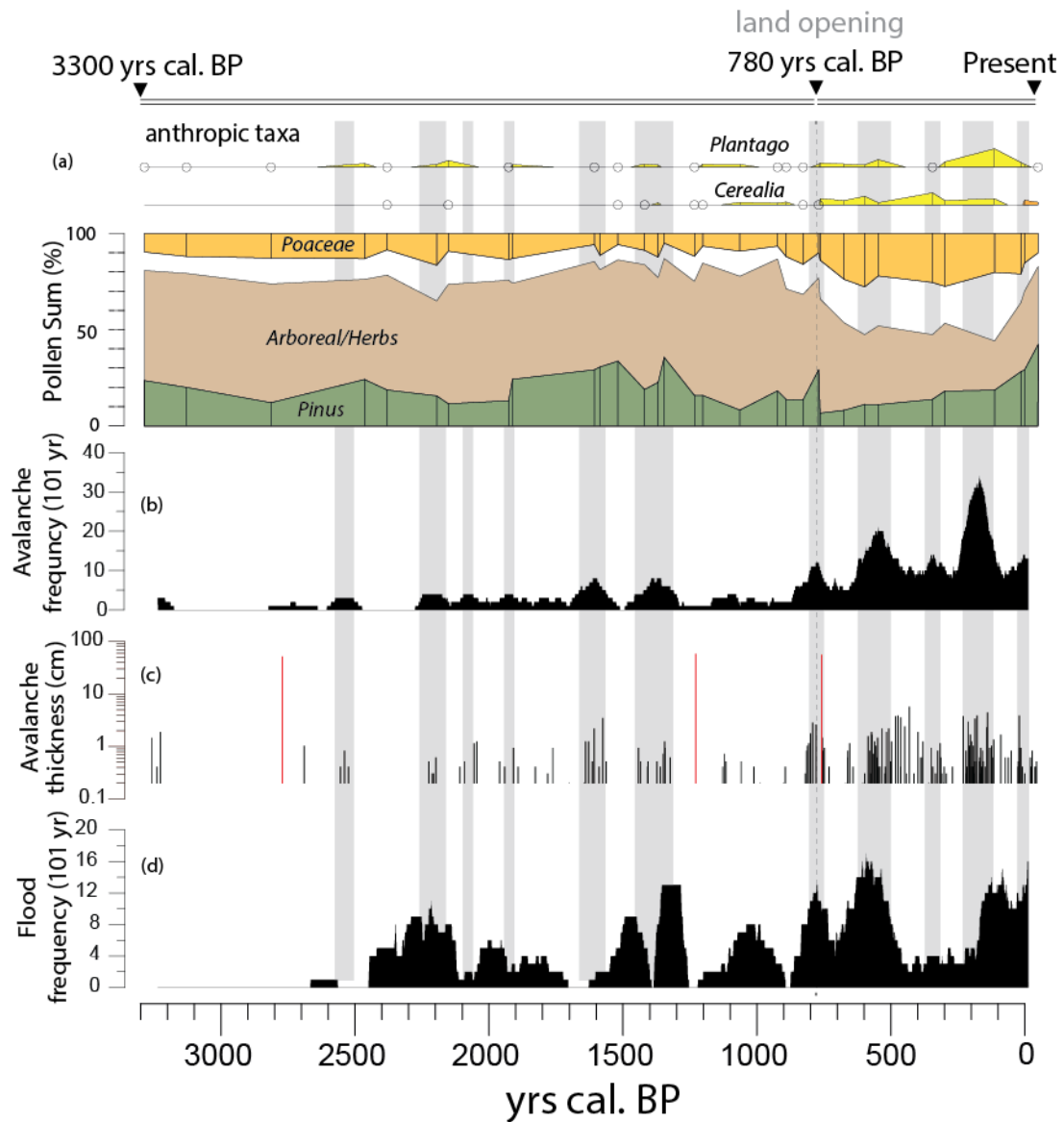
Figure 7: Lake Lauvitel extreme event erosion pattern versus pollen data. (a) Anthropic taxa found in pollen analysis, and pollen sum (%) of Poaceae, Pinus, and ratio between Arboreal/Herbs pollen. (b) Lauvitel avalanche chronicle averaged on 101 year. (c) Lake Lauvitel avalanche thickness in centimeters (red bars correspond to the three thickest avalanche deposits). (d) Lake Lauvitel flood chronicle (averaged on a 101 year). Grey band indicate periods of higher avalanche activity.
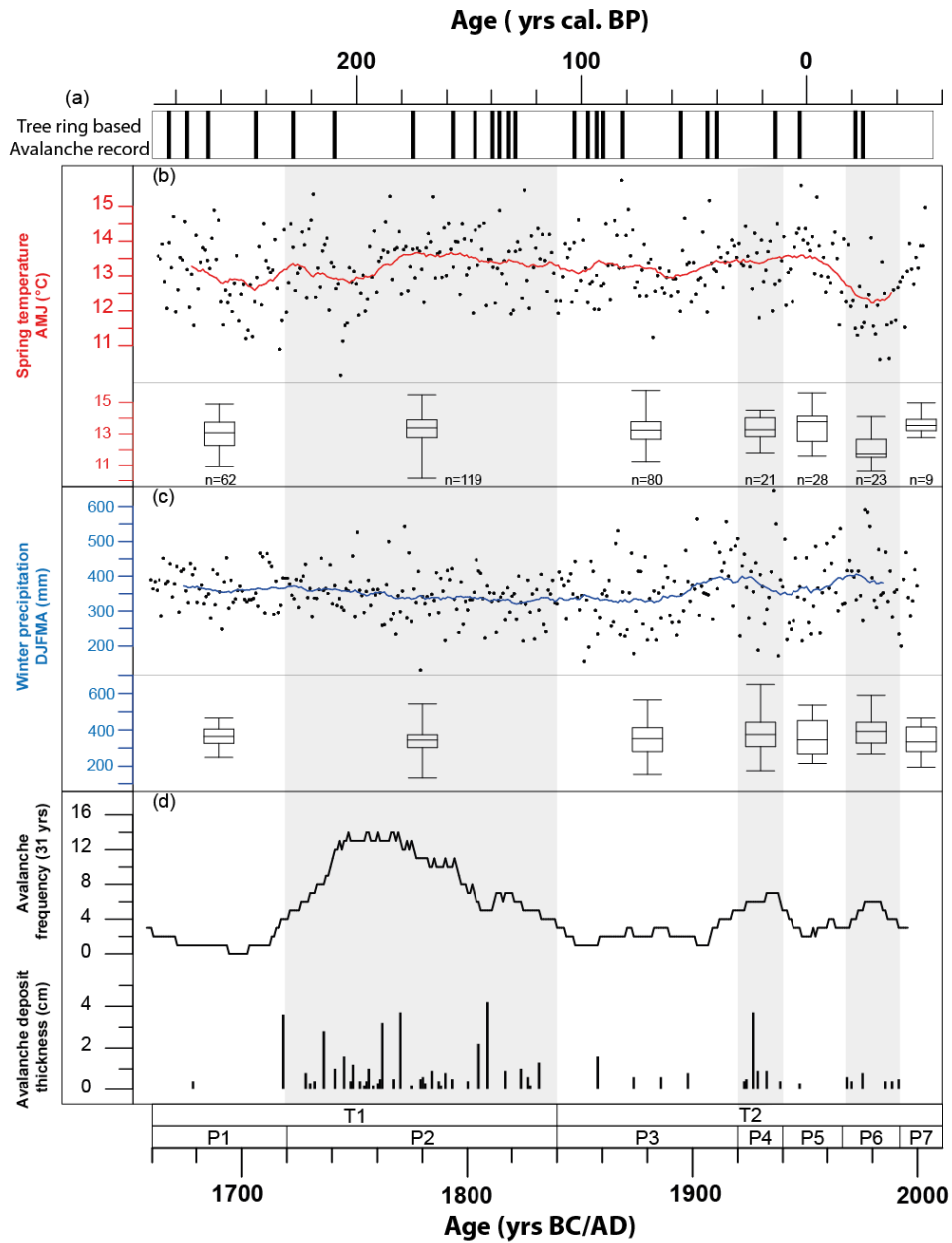
Figure 8: Comparison between Lake Lauvitel avalanche record and climate parameters on the last 350 years. a) Tree ring based avalanche record from Corona et al., (2013); b) spring temperature (AMJ) record (on a 31 yr average in red) and c) winter precipitation DJFMA (mm) (on a 31 yr average in blue) based on instrumental and documentary proxy data on a montly basis from Casty et al., (2005). Data are summarized in box whisker plots corresponding to each identified period (P1 to P7). d) Lake Lauvitel avalanche frequency and avalanche deposit thickness. Grey bands indicate period of higher avalanche frequency.
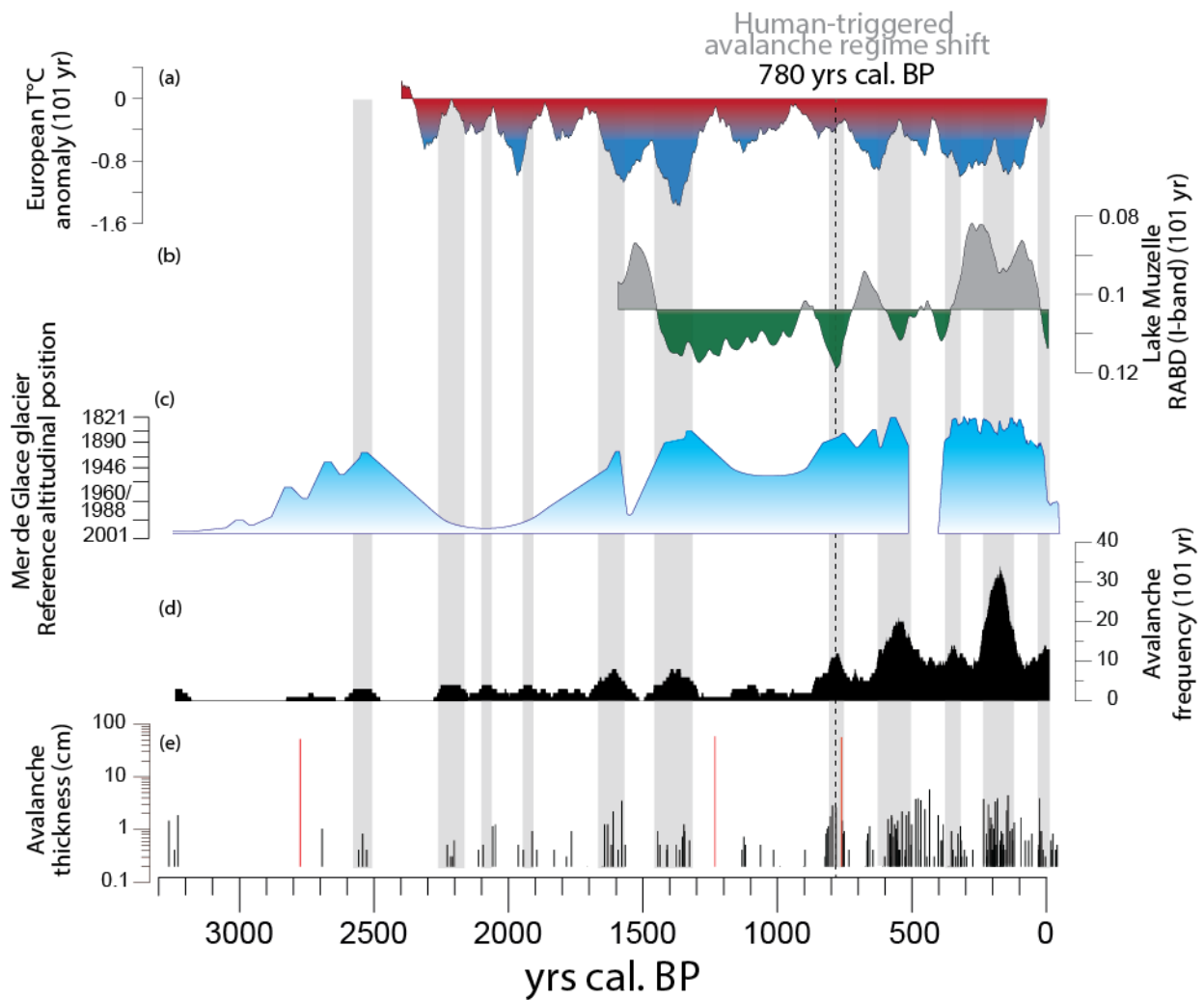
Figure 9: Lake Lauvitel avalanche record compared to climate paramaters. (a) European temperature anomaly from Büntgen et al., (2011), (b) nearby Muzelle glacier fluctuation (Fouinat et al., 2017b), (c) the Mer de Glace length record from Le Roy et al., (2015), (d) Lauvitel avalanche frequency on a 101 yrs average, and (e) avalanche thickness (cm).

Table 1: Radiocarbon ages for LAU11 sediment sequence. Bold samples are excluded dates in the age model.

Sample name	Lab. Code	Depth (cm)	Sample type	^{14}C yr BP			BP range (cal.)	Prob.
LAU1102A-1	Poz-57964	188	Twig	150	±	30	0-283	95
LAU1101E1-1	Poz-55504	247	Twig	145	±	30	3-284	95
LAU1101B-1	Poz-55502	339	Twig	325	±	30	307-468	95
LAU1101D1-1	Poz-55503	617	Twig	850	±	30	691-896	95
LAU1101D2-1	Poz-57963	729	Twig	915	±	30	764-919	95
LAU1101B-1	Poz-55501	923	Twig	1435	±	30	1296-1378	95
LAU1101E1-1	Poz-57955	924	Plant macroremains	1500	±	35	1310-1531	95
LAU1101E1-2	Poz-57956	1000	Leaf	1490	±	30	1307-1513	95
LAU1101E2-1	Poz-57958	1032	Plant macroremains	1725	±	30	1305-1704	95
LAU1101E2-2	**Poz-55505**	**1108**	**Twig**	**1875**	**±**	**30**	**1728-1879**	**95**
LAU1101F1-1	Poz-54236	1245	Plant macroremains	2080	±	30	1953-2138	95
LAU1101F1-2	Poz-54237	1290	Plant macroremains	2270	±	30	2160-2348	95
LAU1101F1-3	Poz-57959	1335	Roots	2150	±	30	2010-2304	95
LAU1101F1-4	Poz-54238	1380	Twig	2215	±	35	2324-2150	95
LAU1101F2-1	Poz-57960	1412	Tree bark	2400	±	30	2348-2678	95
LAU1101F2-2	**Poz-54239**	**1445**	**Twig**	**2990**	**±**	**30**	**3069-3321**	**95**
LAU1101F2-3	Poz-57962	1468	Plant macroremains	2600	±	30	2716-2811	95
LAU1101G-1	Poz-54240	1516	Leaf	2925	±	30	2975-3163	95
LAU1101G-2	Poz-59792	1546	Plant macroremains	3070	±	35	3182-3366	95